Quantitative calculation of the spatial extension of the Kondo cloud

Gerd Bergmann*
Department of Physics, University of Southern California, Los Angeles, California 90089-0484, USA
(Received 7 November 2007; published 4 March 2008)

A recently developed compact solution for the singlet state of the Friedel-Anderson and the Kondo impurity is applied to investigate the old question of a Kondo cloud in the Kondo ground state. Wilson's states with an exponentially decreasing frame of energy cells toward the Fermi level are used. The Wilson states are expressed as free electron waves with a linear dispersion and integrated over the width of their energy cells. For the magnetic state of the Friedel-Anderson impurity, one finds essentially no spin polarization in the vicinity of the *d* impurity. However, for the magnetic *component* of the singlet state, a spin polarization cloud is observed which screens the spin (magnetic moment) of the *d* electron. The range ξ_K of this polarization cloud is investigated in detail for the Kondo impurity. The range is inversely proportional to the Kondo energy Δ_K. The extent of the electron density in real space is a detector for a resonance in energy. The spatial extension ξ and the resonance width Δ are reciprocal and given by the relation $\xi\Delta \approx \hbar v_F$.

DOI: 10.1103/PhysRevB.77.104401 PACS number(s): 75.20.Hr, 71.23.An, 71.27.+a

I. INTRODUCTION

The properties of magnetic impurities in a metal is one of the most intensively studied problems in solid state physics. The work of Friedel[1] and Anderson[2] laid the foundation to understand why some transition-metal impurities form a local magnetic moment while others do not. Kondo[3] showed that multiple scattering of conduction electrons by a magnetic impurity yields a divergent contribution to the resistance in perturbation theory. Kondo's paper stimulated a large body of theoretical and experimental work which changed our understanding of *d* and *f* impurities completely (see, for example, Refs. 4–13). A large number of sophisticated methods were applied in the following three decades to better understand and solve the Kondo and Friedel-Anderson problems. In particular, it was shown that at zero temperature, the Friedel-Anderson impurity is in a nonmagnetic state. To name a few of these methods: scaling,[14] renormalization,[15–18] Fermi-liquid theory,[19,20] slave bosons (see, for example, Ref. 21), and large-spin limit.[22,23] After decades of research, exact solutions of the Kondo and Friedel-Anderson impurities were derived with help of Bethe ansatz,[24–26] representing a magnificent theoretical achievement. The experimental and theoretical progress has been collected in a large number of review articles.[7–13,15,20,21,23–27]

One of the most controversial aspects of the Kondo ground state is the so-called Kondo cloud within the radius ξ_K, where ξ_K is called the Kondo length,

$$\xi_K = \frac{\hbar v_F}{k_B T_K} \tag{1}$$

($k_B T_K = \varepsilon_K$=Kondo energy and v_F=Fermi velocity of the *s* electrons).

The idea is to divide the ground state Ψ_K of a Kondo impurity into two parts with opposite *d* spins. (By reversing all spins, one can transform one component into the other one.) The proponents of the Kondo cloud argue that in each component, there is an *s* electron within the Kondo sphere which compensates the *d* spin. This *s* electron forms a singlet state with the *d* spin. An important assumption of the Kondo-cloud proponents is that, above the Kondo temperature, the bond is broken and this screening cloud evaporates from the Kondo sphere.

Already in the 1970s, there were a number of theoretical papers with different predictions about the Kondo cloud which stimulated several experimental investigations. In most of the experiments, nuclear magnetic resonance (NMR) was used, for example, in Cu samples with dilute Fe-Kondo impurities. (For details, see Ref. 28 which contains also an overview of the theoretical predictions at that time.) By applying a magnetic field (small enough so that it does not destroy the Kondo singlet state), NMR was used to measure the electron spin polarization at shells of Cu atoms around the Fe impurity. The line shift (adjusted with the temperature dependent susceptibility of the Fe impurity) did not show any change when the temperature crossed the Kondo temperature. This contradicted the concept that, in the Kondo ground state, the *d* impurity was paired with and screened by an *s* electron which evaporates above the Kondo temperature.

In recent theoretical papers, the argument is made that an NMR experiment cannot possibly detect the screening electron because of the large volume of the Kondo sphere. With a radius of the order of 0.1 μm (or larger), the Kondo sphere contains more than 2.0×10^8 atoms. Then, the Kondo cloud is only a faint Kondo fog. It is spread so thinly that the change of polarization felt by an individual Cu atom cannot be detected in an NMR experiment.

Actually, the experimental side has not improved so far but a number of theoretical suggestions have been published since 2000 which propose to observe the Kondo cloud in submicron structures, in particular, in connection with quantum dots.[29–33] A number of these papers also contain numerical renormalization calculation to obtain the correlation functions between the impurity spin and the spin of the conduction electrons.

In this paper, I calculate quantitatively the screening cloud of a Friedel-Anderson and a Kondo impurity in the magnetic and the singlet state.

The paper is organized as follows. In Sec. II, the theoretical background of this paper will be introduced, the Friedel

artificially inserted resonance (FAIR) method (in combination with the use of Wilson states). In Sec. III, the numerical results for the spatial density of the s electrons will be reported and analyzed for several cases. First, the spatial extent of the simple Friedel d resonance with spinless electrons is discussed. Since the physics of the Friedel impurity is simple, this consideration will give us confidence in the use of the Wilson wave functions. In the next step, the electronic environment of the Friedel-Anderson (FA) impurity is investigated. The calculation is first performed for its magnetic state. The latter represents the magnetic building block of the singlet ground state of the FA impurity which is investigated next. Last but not the least, the ground state of the Kondo Hamiltonian is analyzed. The subtle modification between the magnetic and the singlet ground state is discussed. Section IV contains the conclusion. Details of the FAIR states, the numerical procedure and the Wilson states are presented in the Appendix, including the wave functions of the Wilson states and their density in real space.

II. THEORETICAL BACKGROUND

A. Friedel artificially inserted resonance method

To investigate the question of a Kondo cloud, I first consider a Friedel-Anderson impurity with spin 1/2 in a metal host. The underlying Hamiltonian consists of two Friedel resonance Hamiltonians (one for each spin) and a Coulomb term $Un_{d,\uparrow}n_{d,\downarrow}$,

$$H_{FA} = \sum_{\sigma} \left\{ \sum_{\nu=1}^{N} \varepsilon_{\nu} c_{\nu\sigma}^{\dagger} c_{\nu\sigma} + E_d d_{\sigma}^{\dagger} d_{\sigma} + \sum_{\nu=1}^{N} V_{sd}(\nu)[d_{\sigma}^{\dagger} c_{\nu\sigma} + c_{\nu\sigma}^{\dagger} d_{\sigma}] \right\} + U n_{d,\uparrow} n_{d,\downarrow}. \quad (2)$$

Here, $c_{\nu\sigma}^{\dagger}$ represent the creation operators of the Wilson s-electron state (which are discussed in Appendix C), $d_{\sigma}^{\dagger}$ represents the creation operator of the d state at the impurity, and $n_{d,\sigma}$ are the operators of the d occupation.

In the Appendixes, I briefly describe the development of a very compact solution for the magnetic state and the singlet state. It uses two localized s states $a_{0+}^{\dagger}$ and $a_{0-}^{\dagger}$ as artificial Friedel resonance states or FAIR states. The ground-state solutions in terms of the FAIR basis have been studied in recent years for the Friedel Hamiltonian,[34,35] the magnetic and the singlet states of the Friedel-Anderson Hamiltonian,[36,37] and the Kondo Hamiltonian.[38] The compact and explicit form makes these solutions ideal for calculation of spatial properties. The compact ground states which are used in this paper are given for the Friedel impurity by Eq. (5), the magnetic state by Eq. (3), the singlet state of the FA impurity by Eq. (4), and the Kondo ground state by Eq. (6).

From the two FAIR states, one can construct uniquely to full bases $\{a_{i+}^{\dagger}\}$ and $\{a_{i-}^{\dagger}\}$. The potentially magnetic state Ψ_{MS} of the Friedel-Anderson Hamiltonian (which is the building block for the singlet state Ψ_{SS}) can be expressed in terms of these new bases,

$$\Psi_{MS} = [A_{s,s} a_{0+\uparrow}^{\dagger} a_{0-\downarrow}^{\dagger} + A_{s,d} a_{0+\uparrow}^{\dagger} d_{\downarrow}^{\dagger} + A_{d,s} d_{\uparrow}^{\dagger} a_{0-\downarrow}^{\dagger} + A_{d,d} d_{\uparrow}^{\dagger} d_{\downarrow}^{\dagger}] \prod_{i=1}^{n-1} a_{i+\uparrow}^{\dagger} \prod_{i=1}^{n-1} a_{i-\downarrow}^{\dagger} \Phi_0. \quad (3)$$

The magnetic state Ψ_{MS} has the same structure as the mean-field solution Ψ_{mf}.[36] The only difference is that the state Ψ_{MS} opens a wide playing field for optimization. (i) The FAIR states $a_{0+}^{\dagger}$ and $a_{0-}^{\dagger}$ can be individually optimized, each one defining a whole basis $\{a_{i\pm}^{\dagger}\}$ [which yields a Hamiltonian of the form in Fig. 10(a) in the Appendixes]. (ii) The coefficients $A_{\alpha,\beta}$ can be optimized as well, fulfilling only the normalization condition $A_{s,s}^2 + A_{d,s}^2 + A_{s,d}^2 + A_{d,d}^2 = 1$. This yields a good treatment of the correlation effects. The optimization procedure is described in detail in Ref. 36 and in Appendix B. The state is denoted as the (potentially) magnetic state Ψ_{MS}. It is expected to be a good solution above the Kondo temperature.

The Coulomb interaction in the Friedel-Anderson impurity destroys the symmetry between the occupation of spin up and down electrons and generates a magnetic moment (if U is large enough). However, this state with broken symmetry is degenerate. Its counterpart with reversed spins has the same energy, and at zero temperature, the two form a new symmetric state which has a different symmetry than the original one. This is somewhat analogous to an atom in a harmonic potential. If some process transforms the harmonic potential into a double well potential, then the atom has an energy minimum on either the left or the right side. Each state breaks the symmetry. However, the new ground state is a symmetric superposition of left and right occupations, yielding a new symmetric state.

In a similar way, I use the magnetic state as a building block for the singlet ground state. Ψ_{MS} together with its counterpart where all spins are reversed yield two states $\bar{\Psi}_{MS}(\uparrow\downarrow)$ and $\bar{\bar{\Psi}}_{MS}(\downarrow\uparrow)$. The singlet ground state is then given by

$$\Psi_{SS} = \bar{\Psi}_{MS}(\uparrow\downarrow) \pm \bar{\bar{\Psi}}_{MS}(\downarrow\uparrow),$$

$$\Psi_{SS} = [\overline{A_{s,s}} a_{0+\uparrow}^{\dagger} a_{0-\downarrow}^{\dagger} + \overline{A_{s,d}} a_{0+\uparrow}^{\dagger} d_{\downarrow}^{\dagger} + \overline{A_{d,s}} d_{\uparrow}^{*} a_{0-\downarrow}^{\dagger} + \overline{A_{d,d}} d_{\uparrow}^{\dagger} d_{\downarrow}^{\dagger}] \prod_{i=1}^{n-1} a_{i+\uparrow}^{\dagger} \prod_{i=1}^{n-1} a_{i-\downarrow}^{\dagger} \Phi_0 \pm [\overline{\bar{A}_{s,s}} a_{0+\downarrow}^{\dagger} a_{0-\uparrow}^{\dagger} + \overline{\bar{A}_{s,d}} a_{0+\downarrow}^{\dagger} d_{\uparrow}^{\dagger} + \overline{\bar{A}_{d,s}} d_{\downarrow}^{\dagger} a_{0-\uparrow}^{\dagger} + \overline{\bar{A}_{d,d}} d_{\uparrow}^{\dagger} d_{\downarrow}^{\dagger}] \prod_{i=1}^{n-1} a_{i+\downarrow}^{\dagger} \prod_{i=1}^{n-1} a_{i-\uparrow}^{\dagger} \Phi_0 \quad (4)$$

(If all spin up states are moved to the left the plus sign applies). The bars on top of Ψ_{MS} are supposed to point out that all the parameters such as $a_{0\pm}^{\dagger}$ and $A_{\alpha,\beta}$ have to be newly optimized. One can set the coefficients $\overline{A_{x,y}}$ and $\overline{\bar{A}_{x,y}}$ as pairwise equal or treat them as independent parameters. The resulting ground states and their energies are identical. (For independent coefficients, one also obtains the triplet state).

At this point, a short summary of the constrain of the state [Eq. (4)] and its numerical solution would be in place. Since the details have been discussed in previous publications, I summarize the construction of the bases $\{a^\dagger_{i\pm}\}$, the different states Ψ_{MS} and Ψ_{SS}, and their numerical optimization in Appendix B.

The resulting ground state is a very good approximation for the exact ground state. Its ground-state energy and the d occupations for zero, one, and two d electrons at the impurity are of the same quality as the best numerical calculations in the field.[39]

III. NUMERICAL RESULTS

A. Friedel impurity

I start the analysis with the Friedel resonance of a spinless d impurity. Since the Friedel Hamiltonian is a single particle Hamiltonian which can be solved exactly, one is here on familiar ground and the interpretation of the results will guide us in the less known territory of the Friedel-Anderson and the Kondo impurity.

We consider a half occupied Wilson band of s electrons with $n=N/2$ electrons, where N is the number of Wilson states. In the absence of the impurity, the n-particle ground state Ψ_0 is given by

$$\Psi_0 = \prod_{\nu=0}^{n-1} c^\dagger_\nu \Phi_0,$$

where $c^\dagger_\nu$ are the creation operators of the Wilson states.

A (spinless) Friedel d impurity is introduced at the position $x=0$. This impurity has an s-d interaction with the states $\psi_\nu(x)=\langle c^\dagger_\nu \Phi_0 | x\rangle$. Due to the impurity, the n-electron state Ψ_0 is modified. As discussed in the Appendixes, the exact ground state of the Friedel impurity can be written as

$$\Psi_F = (Aa^\dagger_0 + Bd^\dagger)\prod_{i=1}^{n-1} a^\dagger_i \Phi_0. \tag{5}$$

The composition of the FAIR state $a^\dagger_0$ and the coefficients A and B are obtained by an iteration process in which the FAIR state is rotated in Hilbert space into its optimal orientation. Details of this iteration process and the construction of the full ground state have been described in previous papers[34,37] and are summerized in Appendix B.

In the next step, we have to calculate the integrated electron density in the presence of the Friedel d impurity at the origin. This calculation is discussed in Appendix C. The density of the state $\psi_\nu(x)$ is given by

$$\rho^0_\nu(x) = |\psi_\nu(x)|^2 = 2^{\nu+3}\frac{\sin^2\left(\pi x \frac{1}{2^{\nu+2}}\right)}{\pi x}$$

for $\nu < N/2$. In the evaluation, we use $N=50$ Wilson states. From the above equation, one recognizes that the main contribution to the density ρ^0_ν of the state ψ_ν lies roughly in the region $|x| < 2^{\nu+2}$ (in units of $\lambda_F/2$). Since for negative energies ν takes the values from 0 to $(N/2-1)$, the different wave functions $\psi_\nu(x)$ have very different spatial ranges and therefore very different densities, the lowest being of the order of $2^{-25} < 3\times 10^{-8}$. Therefore, one has to be careful in the summation of the different contributions.

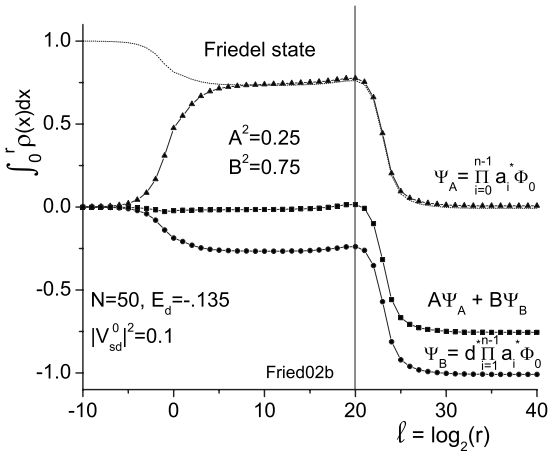

FIG. 1. The net integrated density $\int_0^r \rho(x)dx$ is plotted versus the logarithm of the distance $l=\log_2(r)$ from the impurity for the components Ψ_A, Ψ_B and the full wave function Ψ_F. For the dotted line, the additional one d electron has been added.

In the numerical evaluation, we calculate (i) the s-electron density in the presence and absence of the d impurity, (ii) form the net s-electron density $\rho(x)$ as the difference, and (iii) integrate the net s-electron density from $x=0$ to r, where r is increased on an exponential scale, $r=2^l$, and plot the net integrated s-electron density versus $l=\log_2(r)$.

For the numerical calculation, I use the parameters of $|V^0_{sd}|^2=0.1$ and $E_d=-0.135$. The resulting net integrated density $q(r)=\int_0^r \rho(x)dx$ is plotted in Fig. 1 as a function of the (logarithm of the) distance $\log_2(r)$ from the impurity. The full triangles, circles, and squares give the integrated net s-electron density for the two components $\Psi_A=\Pi_{i=0}^{n-1} a_i^\dagger \Phi_0$ and $\Psi_B=d^\dagger \Pi_{i=1}^{n-1} a_i^\dagger \Phi_0$ of the ground state, and for the full ground state Ψ_F. The curve for Ψ_A increases from 0 to 0.75 roughly between $l=-2$ and $+3$. Around $l=23$, it drops back to zero. It has to return to zero because the total number of occupied states in Ψ_A is the same as before in the state $\Psi_0 = \Pi_{i=0}^{n-1} c^\dagger_\nu \Phi_0$, i.e., equal to $n=N/2$. The equivalent distance $r=2^{23}$ corresponds roughly to the maximum range of the wave functions. In a way, it can be considered as the border or surface of the theoretical sample. Therefore, the interpretation of this curve in Fig. 1 is that in the state Ψ_A, a fraction of 0.75 electrons has moved from the surface toward the d impurity. There it surrounds the empty d state in the spatial region between $r=2^{-2}$ and 2^3. (The component Ψ_A has no d electron.) The behavior of the integrated net density beyond about $l\approx 20$ is a surface effect and of no interest for the present investigation. If one increases the number of Wilson states from N to N', then this part of the curve moves by $(N'-N)/2$ to the right, while the left part of the curve remains unchanged.

The full circles in Fig. 1 give the change of the net integrated density of s electrons for the state Ψ_B as a function of distance. At large distances ($r\approx 2^{23}$), it approaches the value

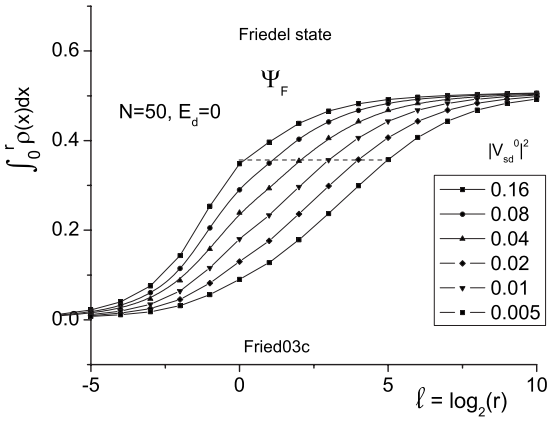

FIG. 2. The net integrated density $\int_0^r \rho(x)dx$ for the state $\Psi_A = \Pi_{i=0}^{n-1} a_i^\dagger \Phi_0$ for different values of $|V_{sd}^0|^2$ and $E_d=0$. The width of the wave function increases proportional to $1/\pi|V_{sd}^0|^2$.

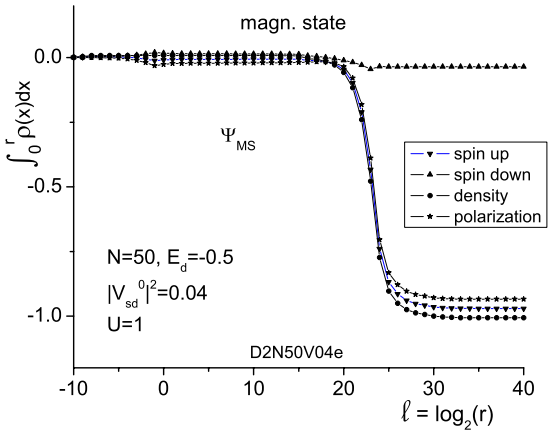

FIG. 3. (Color online) The net integrated density $\int_0^r \rho(x)dx$ of the s electron within a distance r from the impurity for spins up and down, as well as total density and spin polarization. The magnetic moment of the impurity is $0.93\mu_B$.

of -1 because this state has only $(N/2-1)$ s electrons. Between the distances $l=-2$ and $+3$, the curve for Ψ_B assumes the value of -0.25. If one adds to the integrated s-electron density the one d electron at the origin, then one obtains the dotted curve which starts on the left at one and approaches zero at large distances. It is interesting to notice that in the range $5<l<20$, the total integrated density of d and s electrons is equal to 0.75 for both wave functions Ψ_A and Ψ_B. This means that both components have accumulated the same charge close to the impurity.

The Friedel resonance is also ideal testing ground for the spatial extension of the wave function. For that purpose, the d state is moved to the Fermi level ($E_d=0$). The half width of the resonance is given by $\Delta=\pi|V_{sd}^0|^2\rho_0$ (ρ_0=density of states). This resonance width introduces an additional length scale into the problem. In the resonance, the d state hybridizes with the s electrons in this energy range of 2Δ. This corresponds to a wave number range of $k_\Delta \approx 2\pi|V_{sd}^0|^2\rho_0$ and therefore a smearing of the wave function over a range $x_\Delta \propto 1/(2\pi|V_{sd}^0|^2\rho_0)$ (V_{sd}^0 is measured in unit of ε_F and x_Δ in units of $\lambda_F/2$).

In the numerical evaluation, I change the value of $|V_{sd}^0|^2$ in steps of two from 0.005 to 0.16. Indeed, one recognizes in Fig. 2 that with decreasing $|V_{sd}^0|^2$, the increase of the integrated net density is stretched over an increasing length scale. Since the horizontal separation of the points by 1 corresponds to a factor of 2 in the length scale, each curve is broader by a factor of 2 than the previous one.

The extent of the net integrated density is only visible when the d-state energy E_d lies at the Fermi level. For $E_d=-0.5$, the electron cloud in real space is hidden. Here, the resolution of the Wilson states is of the order of 0.25–0.5 which is larger than the Friedel resonance. One has to subdivide the Wilson states close the resonance to make the latter visible.

B. Magnetic state

The magnetic state Ψ_{MS} is the building block of the singlet state. Its multielectron state is built from four Slater states and shown in Eq. (3). I calculate the net integrated density of spins up and down, as well as total density and spin polarization in the vicinity of the impurity when it is in the magnetic state. For the present purpose, I choose the parameters $E_d=-0.5$, $|V_{sd}^0|^2=0.04$, $U=1$, and $N=50$. This yields a well developed magnetic moment of $\mu=0.93\mu_B$. The occupation of the different components is $A_{s,s}^2=0.0294$, $A_{s,d}^2=0.0057$, $A_{d,s}^2=0.9355$, and $A_{d,d}^2=0.0294$.

In Fig. 3, the net densities are plotted. As discussed above, the range beyond 2^{20} corresponds to the rim or surface of the sample and is of no interest for the density distribution around the impurity. One recognizes that there is only a negligible polarization of the electron gas in the vicinity of the impurity. The important result of Fig. 3 is that there is no polarization cloud around the magnetic state of the impurity.

C. Singlet state of the Friedel-Anderson impurity

The author derived the compact singlet ground state in Ref. 37. Its form is given in Eq. (4). The singlet state does not have a net spin polarization because of the symmetry between spins up and down. However, the individual components may possess a spin polarization cloud. To investigate this question, one has first to decide how one subdivides the symmetric state of the impurity.

In the following analysis of the singlet state Ψ_{SS}, I use the same parameters as for the magnetic state: $E_d=-0.5$, $|V_{sd}^0|^2=0.04$, and $U=1$. This yields the following occupations: $\overline{A_{ss}}^2=0.0146$, $\overline{A_{sd}}^2=0.0028$, $\overline{A_{ds}}^2=0.4629$, and $\overline{A_{dd}}^2=0.0146$. (The double bar occupations are identical). These occupations are very close to half the values of the magnetic state ($A_{s,s}^2=0.0294$, $A_{s,d}^2=0.0057$, $A_{d,s}^2=0.9355$, and $A_{d,d}^2=0.0294$). Therefore, it appears that $\Psi_{ss} \approx (1/\sqrt{2})[\Psi_{MS}(\uparrow\downarrow) + \Psi_{MS}(\downarrow\uparrow)]$. This means that the magnetic state is a robust building blocks of the singlet state. (However, there are subtle changes as we will see below.) Therefore, the spin polarization of one of the magnetic components, for example, of $\overline{\Psi_{MS}(\uparrow\downarrow)}$, would be of interest.

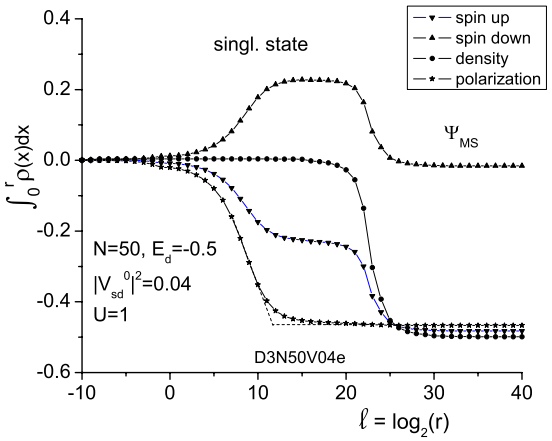

FIG. 4. (Color online) The net integrated density $\int_0^r \rho(x)dx$ within a distance $r=2^l$ from the d-spin up component of the impurity. Shown are the spin up and spin down components as well as the total density and the polarization. The d spin of 0.93/2 is screened by 0.46 s electrons within the range of $r \approx 2^{11.6}$.

In Fig. 4, the integrated densities of spin up and down electrons, their sum, and difference (the polarization) are plotted versus the distance from the magnetic impurity (on a logarithmic scale). One recognizes that now one has considerable contributions to the integrated net densities of both spins. The polarization of the two contributions is no longer zero but reaches a value of −0.46 at a distance of $r \approx 2^{11.6}$. Since the magnetic state with net d-spin up has only a weight of about 1/2, it contributes an effective $d_\uparrow^\dagger$ moment of $0.93/2 \approx 0.46$. Therefore, this d spin is well compensated by the polarization of the s-electron background. The difference with the pure magnetic state is particularly striking. We observe a screening polarization cloud of s electrons about the impurity within the range of $r \approx 2^{11.6} = 3.1 \times 10^3$.

The range of the screening cloud depends on the strength of $|V_{sd}^0|^2$. In Fig. 5, a similar plot as in Fig. 4 is performed for an s-d coupling of $|V_{sd}^0|^2 = 0.1$. This time, the polarization

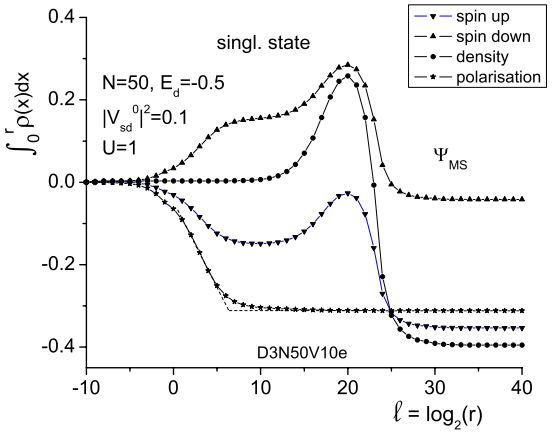

FIG. 5. (Color online) The net integrated density $\int_0^r \rho(x)dx$ within a distance $r=2^l$ form the d-spin up component of the impurity. Shown are the spin up and spin down components as well as the total density and the polarization. The $d_\uparrow$-spin polarization cloud extends for $|V_{sd}^0|^2 = 0.1$ over a range of $r \approx 2^{6.4}$.

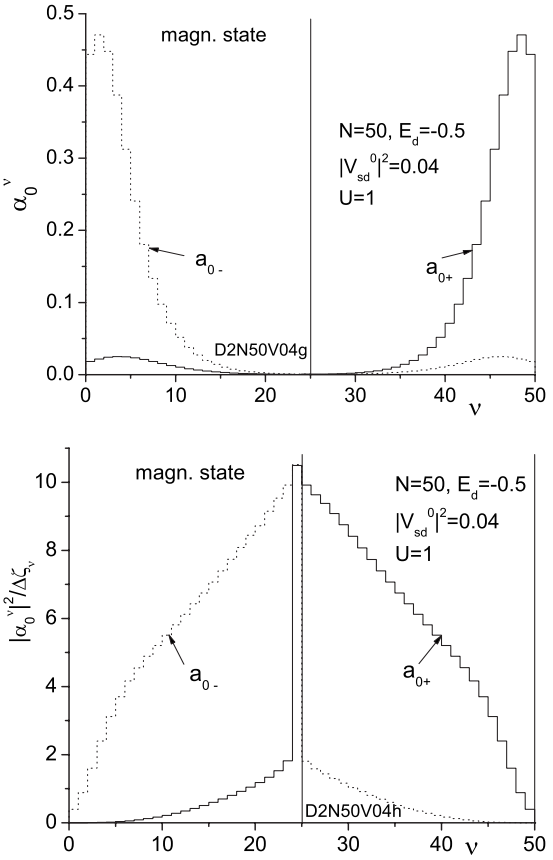

FIG. 6. (a) The coefficients $\alpha_{0\pm}^\nu$ of the FAIR states $a_{0+}^\dagger$ and $a_{0-}^\dagger$ are plotted in terms of the states $c_\nu^\dagger$ for the magnetic state Ψ_{MS}. The full and the dashed curves represent $a_{0+}^\dagger$ and $a_{0-}^\dagger$, respectively. (b) The density distribution of the $p_\nu = |\alpha_{0\pm}^\nu|^2/\Delta_\nu$ as a function of ν.

cloud extends only over a distance of $r \approx 2^{6.4} \approx 84$.

D. Frìedel artifically inserted resonance states

It is remarkable how different the polarizations of the s electrons in the magnetic state Ψ_{MS} and the magnetic component of the singlet state $\overline{\Psi_{MS}}$ are. This is particularly surprising since the amplitudes $\overline{A_{\alpha,\beta}} = \overline{\overline{A}}_{\alpha,\beta}$ in the singlet state are roughly equal to $A_{\alpha,\beta}/\sqrt{2}$. However, in the singlet state, one has a finite coupling between $\overline{\Psi_{MS}}$ and $\overline{\overline{\Psi}}_{MS}$. This affects the composition of the FAIR states $a_{0+}^\dagger$ and $a_{0-}^\dagger$. The two states $a_{0+}^\dagger$ and $a_{0-}^\dagger$ contain the whole information about the many electron states Ψ_{MS} or Ψ_{SS}. When $a_{0\pm}^\dagger$ are known, the whole bases $\{a_{i+}^\dagger\}$ and $\{a_{i-}^\dagger\}$ and the coefficients $A_{\alpha,\beta}$ can be reconstructed. Therefore, it is worthwhile to compare the two FAIR states for the magnetic and the singlet states.

For the magnetic state, the coefficients $\alpha_{0\pm}^\nu$ of the states $a_{0\pm}^\dagger = \Sigma_\nu \alpha_{0\pm} c_\nu^\dagger$ are plotted in Fig. 6 versus the cell number ν, which is a measure of the energy. While $a_{0+}^\dagger$ is essentially concentrated at positive energies, the coefficients of $a_{0-}^\dagger$ have their main weight at negative energies. The two are mirror images with respect to the energy zero.

In Fig. 6(b), the quantity $p_\nu = |\alpha_0^\nu|^2/\Delta_\nu$ is plotted as a function ν, where $\Delta_\nu = (\zeta_{\nu+1} - \zeta_\nu)$ is the width of the energy cell $\mathfrak{C}_\nu$

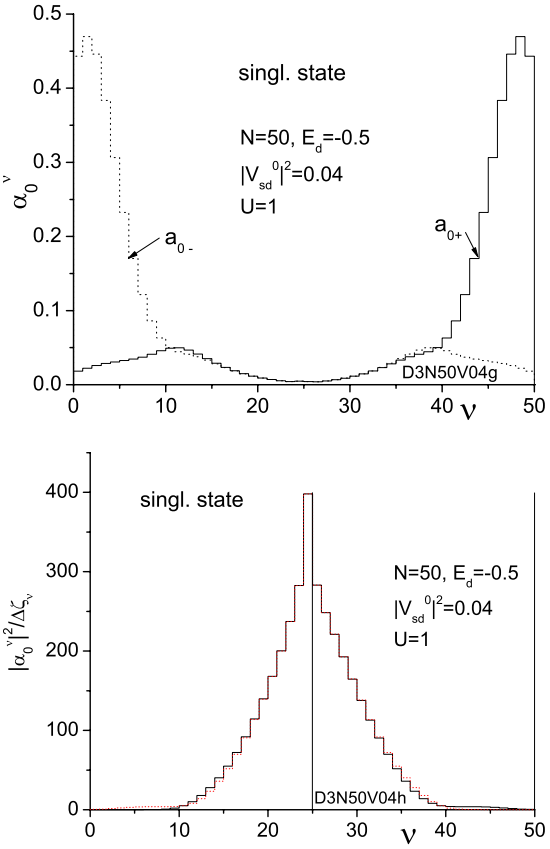

FIG. 7. (Color online) (a) The coefficients $\alpha^{\nu}_{0\pm}$ of the FAIR states $a^{\dagger}_{0+}$ and $a^{\dagger}_{0-}$ in terms of the Wilson states $c^{\dagger}_{\nu}$ of the magnetic component Ψ_{MS} of the singlet state. (b) The density distribution of the $p_{\nu}=|\alpha^{\nu}_{0\pm}|^2/\Delta_{\nu}$ as a function of the cell number ν.

of the Wilson state $\psi_{\nu}(x)$. The quantity p_{ν} is a function of the energy $p_{\nu}=p(\zeta)$, and $p(\zeta)d\zeta$ represents the weight of the original basis states $\varphi_k(x)$ in the energy window $(\zeta,\zeta+d\zeta)$ to the FAIR state $a^{\dagger}_0$. This weight is plotted in Fig. 6(b) for the magnetic state as a function of ν. It would be more natural to plot $p(\zeta)$ as a function of the energy. However, for ν close to $N/2$, the width of the energy cells $\mathfrak{C}_{\nu}$ is less than 10^{-6} and any dependence of $p(\zeta)$ on the energy cannot be resolved on a linear scale. The probability p_{ν} increases close to the Fermi energy. Again, the contributions of $a^{\dagger}_{0+}$ and $a^{\dagger}_{0-}$ resemble mirror images.

In Figs. 7(a) and 7(b), the corresponding plots are shown for the magnetic component of the singlet state. While the overall shape of the coefficients in Fig. 7(a) resembles that in Fig. 6(a), the weight $p_{\nu\pm}=|\alpha^{\nu}_{0\pm}|^2/\Delta_{\nu}$ close to the Fermi level is very different for the singlet state and the magnetic state. While the two probabilities are mirror images for the magnetic case and reach a maximum value of about 10, one observes in the singlet state a maximum of about 400 and the weights $p_{\nu\pm}$ in $a^{\dagger}_{0+}$ and $a^{\dagger}_{0-}$ are essentially identical and not mirror images. The magnetic component of the singlet state is in a subtle way different from the magnetic state.

It is interesting to note that the spatial densities of the two FAIR states $a^{\dagger}_{0+}$ and $a^{\dagger}_{0-}$ (after averaging over Friedel oscillations) are identical with an accuracy of four digits. This

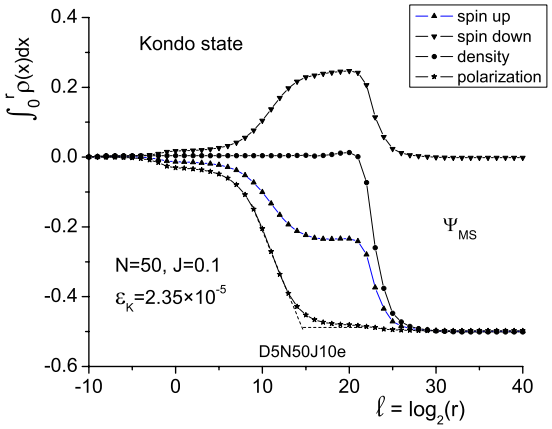

FIG. 8. (Color online) The net integrated density $\int_0^r \rho(x)dx$ within a distance $r=2^l$ from the d-spin up component of the impurity. Shown are the spin up and spin down components as well as the total density and the polarization.

applies for the magnetic and the singlet states. However, their energy expectation values are essentially opposite equal. The values for $\langle a^{\dagger}_{0+}\Phi_0|H|a^{\dagger}_{0+}\Phi_0\rangle$ are rather similar in the magnetic state ($\approx+0.288$) and the singlet ground state ($+0.2865$) of the FA impurity.

E. Kondo impurity

If one increases the Coulomb potential in the Friedel-Anderson impurity (and lowers the d-state energy E_d), then the coefficients $A_{s,s}$ and $A_{d,d}$ converge toward zero. This is the limit of the Kondo impurity. By means of the Schrieffer-Wolff transformation,[40] one can express the s-d interaction as an exchange interaction of the form $2J\mathbf{s}\cdot\mathbf{S}$. In this limit, the compact ground state Ψ_K takes the form

$$\Psi_K=[\overline{A_{s,d}}a^{\dagger}_{0+\uparrow}d^{\dagger}_{\downarrow}+\overline{A_{d,s}}d^{\dagger}_{\uparrow}a^{\dagger}_{0-\downarrow}]\prod_{i=1}^{n-1}a^{\dagger}_{i+\uparrow}\prod_{j=1}^{n-1}a^{\dagger}_{j-\downarrow}\Phi_0+[\overline{\overline{A_{d,s}}}a^{\dagger}_{0-\uparrow}d^{\dagger}_{\downarrow}+\overline{\overline{A_{s,d}}}d^{\dagger}_{\uparrow}a^{\dagger}_{0+\downarrow}]\prod_{i=1}^{n-1}a^{\dagger}_{i-\uparrow}\prod_{j=1}^{n-1}a^{\dagger}_{j+\downarrow}\Phi_0. \quad (6)$$

Since Eq. (6) is a reduced form of Eq. (4), the calculation of the integrated net density is analogous to the previous calculation. The Kondo singlet state is composed of two magnetic components represented by the first and the second terms. Note that the effective moment of these magnetic building blocks is less than $1\mu_B$.

We investigate the Kondo ground state for the exchange parameter $J=0.1$ and $J=0.08$. In a recent investigation,[38] we obtained for the coupling of $J=0.1$ a relaxed singlet-triplet excitation (Kondo) energy of $\varepsilon_K(0.1)=2.35\times10^{-5}$ and for $J=0.08$ an $\varepsilon_K(0.08)=1.37\times10^{-6}$. In Fig. 8, the net integrated density is plotted versus the logarithm of the distance $r=2^l$ for the magnetic component with the d-spin up for $J=0.1$ ($\varepsilon_K=2.35\times10^{-5}$). One recognizes that a spin polarized "cloud" (stars) extends up to a distance of $r=2^{14.7}$ from the Kondo impurity.

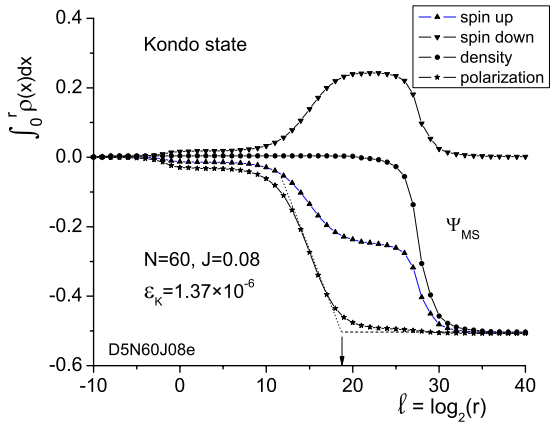

FIG. 9. (Color online) The net integrated density $\int_0^r \rho(x)dx$ within a distance $r=2^l$ from the magnetic component of the impurity. Shown are the spin up and spin down components as well as the total density and the polarization. The polarization extends over a distance of $r=2^{18.8}\approx 4.6\times 10^5(\lambda_F/2)$.

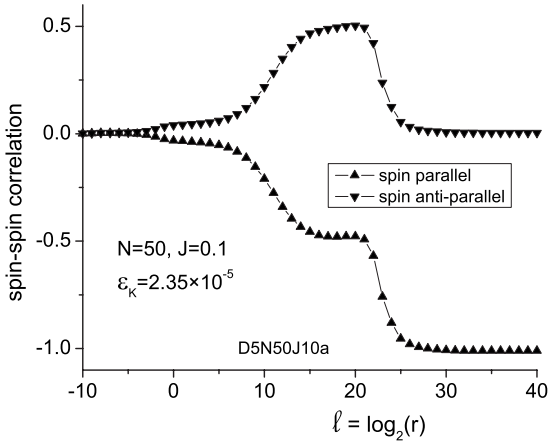

FIG. 10. The spin-spin correlation function (impurity spin is up) for for a Kondo impurity with the same parameters as in Fig. 8.

Next, we want to study the extent of the Kondo cloud as a function of the Kondo energy. By reducing the coupling to $J=0.08$, we observed an $\varepsilon_K(0.08)=1.37\times 10^{-6}$. The ratio of the two energies $\varepsilon_K(0.1)/\varepsilon_K(0.08)$ is equal to 17.1.

Figure 9 shows the integrated net *s*-electron density for a Kondo impurity with $J=0.08$. The two polarization curves (stars) in Figs. 8 and 9 are very nicely parallel. Therefore, the relative shift of the two curves can be determined very accurately. It is equal to 4.1 in terms of the $\log_2$ scale, which corresponds to a length ratio of $2^{4.1}=17.1$. This is a very good agreement with the ratio of 17.1 of the two Kondo energies. Therefore, we can confirm that the extent of the screening cloud scales with the Kondo energy. Kondo energy and extension in real space are reciprocal.

If in Fig. 9 we extrapolate the range of the Kondo cloud as the intersection between the linear decrease and the saturation at the right, then we obtain an intersection of $l=18.8$ or a range of $2^{18.8}$ (in units of $\lambda_F/2$). In the reduced length units of $\lambda_F/2$ and the energy units of ε_F, the Kondo length [Eq. (1)] has the values $\xi_K=2/(\pi\varepsilon_K)$, where ε_K is the Kondo energy in units of ε_F. For the parameters of Fig. 9 ($J=0.08$), the Kondo energy has the value $\varepsilon_K=\Delta E_{st}=1.37\times 10^{-6}$. This yields $\xi_K=4.6\times 10^5\approx 2^{18.8}$. The perfect agreement with the numerical extrapolation is probably lucky because Eq. (1) for the Kondo length is intended as an order of magnitude.

In the analysis of the Kondo impurity, one is often interested in the spin-spin correlation function. This means one subdivides the solution into two parts with impurity spins up and down. One normalizes the part of the wave function with impurity spin up and determines the density of the conduction electrons with parallel and antiparallel spins. If one wants to calculate these densities for the impurity spin up in Eq. (6), then one has to add a rather extensive calculation because one has to include the interference of the charge density between the two terms $d_\uparrow^\dagger a_{0-\downarrow}^\dagger \Pi_{i=1}^{n-1} a_{i+\uparrow}^\dagger \Pi_{j=1}^{n-1} a_{j-\downarrow}^\dagger \Phi_0$ and $d_\uparrow^\dagger a_{0+\downarrow}^\dagger \Pi_{i=1}^{n-1} a_{i-\uparrow}^\dagger \Pi_{j=1}^{n-1} a_{j+\downarrow}^\dagger \Phi_0$. However, for the two examples in Figs. 8 and 9, the occupation of the second term is less than 1/100th of the first term and the interference is further reduced by the fact that the multiscalar product between the two states is of the order of 10^{-2}. Therefore, neglecting the interference introduces only an error of less than 10^{-2}.

In Fig. 10, the spin-spin correlation function is plotted for same the Kondo impurity which is shown in Fig. 8. In this plot the interference is neglected.

IV. CONCLUSION

A recently developed compact solution for the singlet state of the Friedel-Anderson and the Kondo impurity is used to investigate the old question of a Kondo cloud in the Kondo ground state. Wilson's states with an exponentially decreasing frame of energy cells toward the Fermi level and a linear dispersion relation are expressed in free electron waves integrated over the width of their energy cells. A rotational iteration process (which has been described in previous papers) is used to obtain the optimal ground state. The singlet state of the Friedel-Anderson impurity consists of eight Slater states. They are divided into two groups of four, where each group represents one magnetic component of the singlet state.

After identifying the magnetic components, the real space wave function is evaluated. Since the spatial range of the Wilson states varies in the range between a Fermi wave length λ_F and $2^{N/2}\lambda_F$ ($N\approx 50$ is the number of Wilson states used in the evaluation), one has to deal with electron densities which vary be a factor of $2^{25}\approx 3\times 10^7$. Therefore, it is favorable to integrate over the net *s*-electron density from the impurity outward. The resulting curves yield the spatial range over which the spin densities of the *s* electrons contribute to the polarization about the impurity.

If one wants to obtain the polarization about the impurity, then one has to calculate the difference of spin up and down *s*-electron densities with and without the impurity. The simple and exact solution of the Friedel resonance for spinless electrons is used to test the method and interpret the results. It turns out that the behavior of the (integrated) spin densities and polarization can be divided into two regions.

For $r>2^{N/2}$, the system follows the sum rule which is imposed by the number of s and d states in the multielectron Slater state. For $r<2^{N/2}$, one obtains the physical densities and polarizations. The behavior in this range does not change when N is increased.

For a Friedel resonance at the Fermi level, one observes in real space an s-electron cloud whose range is proportional to $1/|V_{sd}^0|^2$.

For the magnetic state Ψ_{MS} of the Friedel-Anderson impurity, one observes essentially no magnetic s polarization in the vicinity of the d impurity.

For the magnetic component $\overline{\Psi_{MS}}$ of the singlet state in the Friedel-Anderson impurity, one observes an s-polarization cloud which screens the spin (magnetic moment) of the d electron. The range of this polarization cloud is investigated in detail for the Kondo impurity. The range is inversely proportional to the Kondo energy. The latter was obtained in a previous investigation as the energy difference between the singlet state and the relaxed triplet state energies. The absolute value of the range of the polarization cloud agrees surprisingly well with the Kondo length.

The different screening behaviors in the magnetic state Ψ_{MS} and the singlet state Ψ_{SS} are due to subtle differences in the composition of the FAIR states $a_{0+}^\dagger$ and $a_{0-}^\dagger$. In the singlet state, the FAIR states have a much larger weight very close to the Fermi energy. It is remarkable that the two FAIR states $a_{0+}^\dagger$ and $a_{0-}^\dagger$, which are far apart in their energy, have essentially an identical density in real space (after averaging over the Friedel oscillations).

In the present paper, a very simple energy band and dispersion relation is used in analogy to Wilson's work. This simplifies the numerical evaluation dramatically. However, the spatial dependence can be evaluated for an arbitrary s band with an energy-dependent density of states and s-d interaction. The author generalized the definition of the Wilson states[41] for this case. The numerical work would, however, be much more extensive.

It should be emphasized that the extent of the Kondo cloud calculated here applies only when the mean free path of the conduction electrons is larger than the Kondo length. Also, the surface of the host should be at least this distance away from the impurity. This does, however, not mean that for smaller sample size the Kondo effect is suppressed. One obtains the full Kondo effect[42] as long as there are sufficiently many electron states within the Kondo resonance which couple to the impurity.

Finally, it should be noted that the extent of the electron density in real space is a detector for a resonance in energy. The spatial extension ξ and the resonance width Δ are reciprocal and given by the relation $\xi\Delta \approx \hbar v_F$. The Wilson states act here as a magnifying glass close to the Fermi energy because their energy width Δ_ν decreases as $2^{-\nu}$ toward the Fermi level. This is particularly demonstrated for the Friedel impurity in Fig. 2. The extent of the net integrated density is only observed when the d-state energy E_d lies at the Fermi level. For $E_d=-0.5$, the electron cloud in real space cannot be detected. Here, the resolution of the Wilson states is of the order of 0.25–0.5 which is not sufficient to detect the Friedel resonance. One has to subdivide the Wilson states close the resonance to make the latter visible. Therefore, the Wilson states can be used as a quasiexperimental spectroscope.

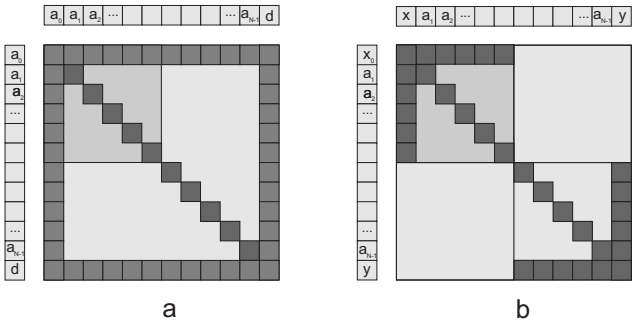

FIG. 11. (a) The matrix of the Friedel Hamiltonian in the basis $\{a_i^\dagger\}$ $d^\dagger$. (b) The two basis vectors $a_0^\dagger, d^\dagger$ are rotated into $x^\dagger=(Aa_0^\dagger+Bd^\dagger)$ and $y^\dagger=(Ba_0^\dagger-Ad^\dagger)$. For the optimal $a_0^\dagger$, the matrix is block diagonal.

APPENDIX A: THE FRIEDEL ARTIFICIALLY INSERTED RESONANCE METHOD

The Hamiltonian of the Friedel-Anderson impurity is given in Eq. (2). One obtains the mean-field Hamiltonian from Eq. (2) by replacing $n_{d+}n_{d-}=>n_{d+}\langle n_{d-}\rangle+\langle n_{d+}\rangle n_{d-}-\langle n_{d+}\rangle\langle n_{d-}\rangle$. After adjusting $\langle n_{d+}\rangle$ and $\langle n_{d-}\rangle$ self-consistently, one obtains two Friedel resonance Hamiltonians with a spin-dependent energy of the d_σ state: $E_{d,\sigma}=E_d+U\langle n_{d,-\sigma}\rangle$,

$$H_{mf}=\sum_\sigma \left\{ \sum_{\nu=1}^{N} \varepsilon_\nu c_{\nu\sigma}^\dagger c_{\nu\sigma} + E_{d\sigma} d_\sigma^\dagger d_\sigma + \sum_{\nu=1}^{N} V_{sd}(\nu)[d_\sigma^\dagger c_{\nu\sigma} + c_{\nu\sigma}^\dagger d_\sigma] \right\}.$$

The mean-field wave function is a product of two Friedel ground states for spins up and down $\Psi_{mf}=\Psi_{F\uparrow}\Psi_{F\downarrow}$.

It has been shown[34,35] that the "exact" n-particle ground state of the Friedel Hamiltonian can be expressed as the sum of two Slater states, in which either the $d^\dagger$ state or a state $a_0^\dagger$ is multiplied with the same $(n-1)$-s-electron state $\prod_{i=1}^{n-1} a_i^\dagger \Phi_0$.

$$\Psi_F=(Aa_0^\dagger+Bd^\dagger)\prod_{i=1}^{n-1} a_i^\dagger \Phi_0.$$

The state $a_0^\dagger=\Sigma_\nu \alpha_{0,\nu} c_\nu^\dagger$ is a localized state whose components $\alpha_{0,\nu}$ can be obtained analytically[35] or by variation.[34]

In Fig. 11(a), the matrix of the Friedel Hamiltonian in the basis $\{a_i^\dagger\}$ $d^\dagger$ is shown. Only the diagonal elements and the elements along the edges are nonzero. The inner $(N-1)\times(N-1)$ submatrix is diagonalized. This way the state $a_0^\dagger$ determines uniquely the full basis $\{a_i^\dagger\}$. One recognizes that the state $a_0^\dagger$ represents a Friedel artificially inserted resonance state, with similar properties as the state $d^\dagger$. Therefore, I call $a_0^\dagger$ a FAIR state. The use of the FAIR states is at the heart of my approach to the FA and Kondo impurity problems. Therefore, I call this approach the FAIR method.

The structure of the Hamiltonian in Fig. 11(a) can be obtained for an arbitrary state $a_0^\dagger$. There is, however, one opti-

mal state $a_0^\dagger$ which yields the exact n-electron eigenstate Ψ_F and for which the energy expectation value $\langle\Psi_F|H_F|\Psi_F\rangle$ has a minimum. For this state, the two basis vectors $a_0^\dagger$ and $d^\dagger$ can be rotated within their plane into the orthogonal states $x^\dagger=(Aa_0^\dagger+Bd^\dagger)$ and $y^\dagger=(Ba_0^\dagger-Ad^\dagger)$. For the optimized $a_0^\dagger$, the resulting Hamiltonian is block diagonal. This is shown in Fig. 11(b). The upper left block contains the occupied states. Since there is no matrix element between the occupied and the empty blocks the product state $x^\dagger a_1^\dagger a_2^\dagger \cdots a_{n-1}^\dagger \Phi_0=(Aa_0^\dagger+Bd^\dagger)\Pi_{i=1}^{n-1} a_i^\dagger \Phi_0$ is an eigenstate.

For the two Friedel states in the mean-field wave function, I use the form of Eq. (5) and obtain for the mean-field solution,

$$\Psi_{mf}=\left[(A_+a_{0+\uparrow}^\dagger+B_+d_\uparrow^\dagger)\prod_{i=1}^{n-1}a_{i+\uparrow}^\dagger\right]\left[(A_-a_{0-\downarrow}^\dagger+B_-d_\downarrow^\dagger)\prod_{i=1}^{n-1}a_{i-\downarrow}^\dagger\right]\Phi_0, \tag{A1}$$

where $\{a_{i+}^\dagger\}$ and $\{a_{i-}^\dagger\}$ are two (different) bases of the N-dimensional Hilbert space. This solution can be rewritten as Eq. (3).

In the mean-field solution Ψ_{mf} the coefficients $A_{\alpha,\beta}$ are restricted by two conditions $A_\pm^2+B_\pm^2=1$ (here, $A_{s,s}=A_+A_-$, etc.). Therefore, this state does not describe well the correlation effects.

In contrast, state (3) opens a wide playing field for improving the solution. (i) The FAIR states $a_{0+}^\dagger$ and $a_{0-}^\dagger$ can be individually optimized, each one defining a whole basis $\{a_{i\pm}^\dagger\}$ [which yields a Hamiltonian of the form in Fig. 11(a)] and (ii) the coefficients $A_{\alpha,\beta}$ can be optimized as well fulfilling only the normalization condition $A_{s,s}^2+A_{d,s}^2+A_{s,d}^2+A_{d,d}^2=1$. This yields a much better treatment of the correlation effects. The resulting state is denoted as the (potentially) magnetic state Ψ_{MS}. The magnetic state Ψ_{MS} has the same structure as the mean field solution Ψ_{mf}; the only difference is that its components are optimized for the Friedel-Anderson Hamiltonian. The optimization procedure is described in detail in Ref. 36 and below in Appendix B.

The magnetic state Ψ_{MS} is used as the building block for the singlet state. Its form is given in Eq. (4).

APPENDIX B: NUMERICAL PROCEDURE

1. Construction of the bases $\{a_{i+}^\dagger\}$ and $\{a_{i-}^\dagger\}$

The construction of the two bases $\{a_{i+}^\dagger\}$ and $\{a_{i-}^\dagger\}$ are completely equivalent. Therefore, I skip the plus or minus subscript and discuss the construction of a basis $\{a_i^\dagger\}$. One starts with the s band which consists of a basis of N states $\{c_\nu^\dagger\}$ (for example, Wilson's states). The $d^\dagger$ state is ignored for the moment.

(1) One forms a normalized state $a_0^\dagger$ out of the s states with

$$a_0^\dagger=\sum_{\nu=1}^{N}\alpha_\nu^0 c_\nu^\dagger.$$

The coefficients α_ν^0 can be arbitrary at first. Some reasonable choices are (i) $\alpha_\nu^0=1/\sqrt{N}$ or (ii) $\alpha_\nu^0=\sqrt{2/n}$ for $\nu<n$ and $\alpha_\nu^0=0$ for $\nu\geqslant n$.

(2) $(N-1)$ new basis states $a_i^\dagger$ $(1\leqslant i\leqslant N-1)$ are formed which are normalized and orthogonal to each other and to $a_0^\dagger$.

(3) The s band Hamiltonian matrix H_0 is constructed in this new basis. One puts the state $a_0^\dagger$ at the top. Its matrix elements are H_{0i} and H_{i0}.

(4) The $(N-1)$ sub-Hamiltonian which does not contain the state $a_0^\dagger$ is diagonalized. The resulting Hamilton matrix for the s band then has the form

$$H_0=\begin{pmatrix} E(0) & V_{fr}(1) & V_{fr}(2) & \cdots & V_{fr}(N-1) \\ V_{fr}(1) & E(1) & 0 & \cdots & 0 \\ V_{fr}(2) & 0 & E(2) & \cdots & 0 \\ \cdots & \cdots & \cdots & \cdots & \cdots \\ V_{fr}(N-1) & 0 & 0 & \cdots & E(N-1) \end{pmatrix}. \tag{B1}$$

The creation operators of the new basis are given by a new set of $\{a_i^\dagger\}$ $(0<i\leqslant N-1)$. Again, the $a_i^\dagger$ can be expressed in terms of the s states; $a_i^\dagger=\Sigma_{\nu=1}^N \alpha_\nu^i c_\nu^\dagger$. The state $a_0^\dagger$ determines uniquely the other basis states $a_i^\dagger$. The additional s-d hopping Hamiltonian can be expressed in the terms of the new basis. The state Ψ_{MS} or Ψ_{SS} can be formed. Their general form is

$$\Psi_{FAIR}=\sum_X A_X\Psi_X,$$

where A_X are the coefficients such as $A_{s,s}$ and Ψ_X the corresponding Slater states such as $a_{0+\uparrow}^\dagger a_{0-\downarrow}^\dagger \Pi_{i=1}^{n-1} a_{i+\uparrow}^\dagger \Pi_{i=1}^{n-1} a_{i-\downarrow}^\dagger \Phi_0$.

(5) The energy expectation value of the full Hamiltonian is calculated. It has the form

$$\langle E\rangle=\frac{\sum_{X,X'} A_X A_{X'}\langle\Psi_X|H|\Psi_{X'}\rangle}{\sum_{X,X'} A_X A_{X'}\langle\Psi_X|\Psi_{X'}\rangle}.$$

The coefficients A_X are varied so that $\langle E\rangle$ takes to lowest value for the bases pair $\{a_{i\pm}^\dagger\}$. This is a standard mathematical problem which can be solved by a (nonorthogonal) transformation of the vector (A_X) and the diagonalization of the new Hamiltonian matrix.

(6) The state $a_0^\dagger$ (for each basis $\{a_{i+}^\dagger\}$ and $\{a_{i-}^\dagger\}$) is rotated in the N-dimensional Hilbert space. In each cycle the state $a_0^\dagger$ is rotated in the $(a_0^\dagger, a_{i_0}^\dagger)$ plane by an angle θ_{i_0} for $1\leqslant i_0 \leqslant N-1$. Each rotation by θ_{i_0} yields a new $\overline{a_0}^\dagger$,

$$\overline{a_0}^\dagger=a_0^\dagger\cos\theta_{i_0}+a_{i_0}^\dagger\sin\theta_{i_0}.$$

For each rotation plane $(a_0^\dagger, a_{i_0}^\dagger)$, the optimal $\bar{a}_0^\dagger$ is determined (which yields with the lowest energy expectation value $\langle E\rangle$). This cycle is repeated until one reaches the absolute minimum of the energy expectation value. The procedure is stopped when the expectation value changes by less than 10^{-10} during a full cycle.

The procedure searches for the minimum of the energy $\langle E\rangle$ in a $2(N-1)$-dimensional space. [The number of rotation planes is equal to $2(N-1)$ as are the independent components of $a_{0+}^{\dagger}$ and $a_{0-}^{\dagger}$.]

APPENDIX C: WILSON'S STATES

Wilson considered an s band with constant density of states and the Fermi energy in the center of the band. By measuring the energy from the Fermi level and dividing all energies by the Fermi energy Wilson obtained a band ranging from -1 to $+1$. To treat the electrons close to the Fermi level at $\zeta=0$ as accurately as possible, he divided the energy interval $(-1:0)$ at energies of $-1/2,-1/4,-1/8,\ldots$, i.e., $\zeta_\nu=-1/2^\nu$. This yield energy cells $\mathfrak{C}_\nu$ with the range $\{-1/2^\nu:-1/2^{\nu+1}\}$ and the width $\Delta_\nu=\zeta_{\nu+1}-\zeta_\nu=1/2^{\nu+1}$.

Wilson rearranged the quasicontinuous original electron states $\varphi_k(x)$ in such a way that only one state within each cell $\mathfrak{C}_\nu$ had a finite interaction with the impurity. Assuming that the interaction of the original electron states $\varphi_k(x)$ with the impurity is k independent, this interacting state in $\mathfrak{C}_\nu$ had the form

$$\psi_\nu(x)=\sum_{\mathfrak{C}_\nu}\varphi_k(x)/\sqrt{Z_\nu},$$

where Z_ν is the total number of states $\varphi_k(x)$ in the cell $\mathfrak{C}_\nu$ [$Z_\nu=Z(\zeta_{\nu+1}-\zeta_\nu)/2$, Z is the total number of states in the band]. There are $(Z_\nu-1)$ additional linear combinations of the states φ_k in the cell $\mathfrak{C}_\nu$ but they have zero interaction with the impurity and were ignored by Wilson as they will be within this paper.

The interaction strength of the original basis states $\varphi_k(x)$ with the d impurity is assumed to be a constant v_{sd}. Then, the interaction between the d state and the Wilson states $\psi_\nu(x)$ is given by $V_{sd}(\nu)=V_{sd}^0\sqrt{(\zeta_{\nu+1}-\zeta_\nu)/2}$, where $|V_{sd}^0|^2=\Sigma_k|v_{sd}|^2=\Sigma_\nu|V_{sd}(\nu)|^2$.

1. Wave function of Wilson's states in real space

For the discussion of the wave functions in real space, one has to look a bit closer. We assume a linear dispersion relation between energy and momentum, a constant density of states, and a constant amplitude at $x=0$. Then, the interaction between the original basis states $\varphi_k(x)$ and the d impurity will be constant for all k states. These assumptions are the same as in Wilson's treatment of the Kondo impurity. We define the wave functions $\varphi_k(x)$ in such a way that the results apply for the impurity problem in one, two, and three dimensions.

a. One-dimensional case

Let us start with the one-dimensional problem. Here, we have the impurity at the position zero and the conduction electrons are located in the range between 0 and L. The wave functions $\varphi_k(x)$ have the form $\varphi_k(x)=\sqrt{2/L}\cos(kx)$. There is another set of eigenstates $\overline{\varphi_k(x)}=\sqrt{2/L}\sin(kx)$. These states do not interact with the impurity at the origin. Therefore, they do not have any bearing on the impurity problem.

b. Three-dimensional case

In three dimensions, the free electron states can be expressed as $\varphi_k(x)=Y_l^m(\theta,\phi)j_l(kx)$, where Y_l^m is a spherical harmonics and l and m are the angular momentum and magnetic quantum numbers. $j_l(kx)$ is a spherical Bessel function. Its long range behavior is given by $(1/r\sqrt{2\pi L})\sin(kx-l\pi/2)$. Only the states with the same l as the impurity couple to the impurity. All the other states for different l belong to the group of inert states $\overline{\varphi_k(x)}$.

If one calculates the density of the wave function, integrates in the three-dimensional case over the spherical surface $4\pi r^2$, and averages over short range (Friedel) oscillations, then one obtains the following result.

(a) One-dimensional case: $(2/L)\overline{\cos^2(kx)}=1/L$.

(b) Three-dimensional case: $\rho_k(x)=(2/L)\overline{\sin^2(kx-l\pi/2)}=1/L$.

In both cases, one obtains essentially the same density. Therefore, it is sufficient to use the one-dimensional approach for calculating the density of a Kondo cloud. It is equivalent to the three-dimensional case integrated over the spherical surface.

c. Wave functions in one dimension

While the energy is measured in units of the Fermi energy, the momentum will be measured in units of the Fermi wave number. We assume a linear dispersion relation for $0\leqslant k\leqslant 2$ with

$$\zeta=(k-1).$$

The (almost) continuous states φ_k are given as

$$\varphi_k(x)=\sqrt{\frac{2}{L}}\cos(\pi kx),$$

where L is the length of the one-dimensional box. Since k is measured in units of k_F, the coordinate x gives the position in units of $\lambda_F/2$, where λ_F is the Fermi wave number. The boundary condition $\cos(\pi kL)=0$ yields $k=(\lambda+1/2)/L$. (The maximal value of λ is $2L$ since k is dimensionless then L is also dimensionless.) Therefore, we have $Z=2L$ states in the full band of width 2.

To obtain the Wilson state, we have to sum the states $\varphi_k(\pi kx)$ over all states within an energy cell. If the cell ranges from $(\zeta_\nu:\zeta_{\nu+1})$ corresponding to a k range $(1+\zeta_\nu)<k<(1+\zeta_{\nu+1})$, then we represent all the states in this energy interval by

$$\psi_\nu(x)=\frac{1}{\sqrt{(\zeta_{\nu+1}-\zeta_\nu)L}}\sum_{1+\zeta_\nu<k<1+\zeta_{\nu+1}}\sqrt{\frac{2}{L}}\cos(\pi kx).$$

From $Z_\nu=L(\zeta_{\nu+1}-\zeta_\nu)$ states, we have (according to Wilson) constructed one state $\psi_\nu(x)$ which couples to the impurity.

The same procedure yields $(Z_\nu - 1)$ additional linear combinations of $\varphi_k(x)$ which do not couple with the impurity at the origin. We denote these states as $\overline{\overline{\varphi_k(x)}}$. They are as inert to the impurity as the states $\overline{\varphi_k(x)}$ and will be included in the quasivacuum.

The wave function of the state $c_\nu^\dagger$ has the form for $\nu < N/2$,

$$\psi_\nu(x) = \frac{2\sqrt{2}}{\sqrt{(\zeta_{\nu+1}-\zeta_\nu)}} \frac{\sin\left(\frac{\pi x(\zeta_{\nu+1}-\zeta_\nu)}{2}\right)}{\pi x} \cos\left(\frac{\pi x(2+\zeta_\nu+\zeta_{\nu+1})}{2}\right).$$

For the exponential energy scale, this yields for $\nu < N/2-1$

$$\psi_\nu(x) = 2\sqrt{2^{\nu+2}} \frac{\sin\left(\pi x \frac{1}{2^{\nu+2}}\right)}{\pi x} \cos\left[\pi x\left(1-\frac{3}{2^{\nu+2}}\right)\right]. \tag{C1}$$

Similarly, one obtains for in the positive energy range,

$$\psi_{N-1-\nu}(x) = 2\sqrt{2^{\nu+2}} \frac{\sin\left(\frac{1}{2^{\nu+2}}\pi x\right)}{\pi x} \cos\left[\pi x\left(1+\frac{3}{2^{\nu+2}}\right)\right].$$

The two wave functions $\psi_{N/2-1}$ and $\psi_{N/2}$ are special because their k range is the same as their neighbors $\psi_{N/2-2}$ and $\psi_{N/2+1}$. All four states close to the Fermi level have the same k range of $2^{-N/2-1}$. One has to pay special attention to this complication.

2. Density of the Wilson states in real space

The density of the wave function $\psi_\nu(x)$ is given by

$$|\psi_\nu(x)|^2 = \frac{8}{(\zeta_{\nu+1}-\zeta_\nu)} \frac{\sin^2\left(\frac{\pi x(\zeta_{\nu+1}-\zeta_\nu)}{2}\right)}{(\pi x)^2} \cos^2\left(\frac{\pi x(2+\zeta_\nu+\zeta_{\nu+1})}{2}\right).$$

The density of a single state $\psi_\nu(x)$ is given by the square of the function $\psi_\nu(x)$ in Eq. (C1). This density has a fast oscillating contribution which yields the Friedel oscillations. We are here interested in the density on a much larger scale and average over the fast oscillation (which has a period of the order of 1 in units of $\lambda_F/2$). Then, we obtain for the Wilson states for $\nu < N/2$, where $(\zeta_{\nu+1}-\zeta_\nu) = \frac{1}{2^{\nu+1}}$,

$$\rho_\nu^0(x) = |\psi_\nu(x)|^2 = 2^{\nu+3} \frac{\sin^2\left(\pi x \frac{1}{2^{\nu+2}}\right)}{(\pi x)^2}. \tag{C2}$$

In the numerical calculation, we will use (most of the time) $N=50$ Wilson states. The different wave functions $\psi_\nu(x)$ have very different spatial ranges and therefore very different densities, the lowest being of the order of $2^{-25} < 3\times 10^{-8}$. This means that it is not useful to calculate the density as a function of x because this density varies over a range of 2^{25}. Instead, we use the integrated density, integrated from 0 to r,

$$q_\nu^0(r) = \int_0^r |\psi_\nu(x)|^2 dx = 2^{\nu+3} \int_0^r \frac{\sin^2\left(\pi x \frac{1}{2^{\nu+2}}\right)}{(\pi x)^2} dx = 2\int_0^{r/2^{\nu+2}} \frac{\sin^2(\pi u)}{(\pi u)^2} du.$$

One realizes that a single integral yields the integrated density for (almost) all wave function $\psi_\nu(x)$. The state $\psi_0(\pi x)$ lies roughly in the range $r < 2^2$, i.e., the integrated density $q_\nu(r) = \int_0^r |\psi_0(x)|^2 dx$ increases in this range to 90%. Therefore, the states $\psi_\nu(x)$ and $\psi_{N-1-\nu}(x)$ essentially lie in the range $r < 2^{\nu+2}$ (in units of $\lambda_F/2$). For a total of $N=50$, Wilson states the maximum range of the wave functions is roughly $2^{N/2-1} = 2^{26}$.

We may define as a ruler a linear array $I(s)$, where s is an integer $(-N/2 \leqslant s < N)$, as

$$I(s) = 2\int_0^{2^s} \frac{\sin^2(\pi u)}{(\pi u)^2} du.$$

Then, the integrated density of the state ψ_ν in the range from 0 to 2^l is given by

$$q_\nu^0(2^l) = \int_0^{2^l} |\psi_\nu(x)|^2 dx = 2\int_0^{2^l/(2^{\nu+2})} \frac{\sin^2(\pi u)}{(\pi u)^2} du = I(l-\nu-2),$$

where $I(l-\nu-2)$ gives the integrated density of the wave function ψ_ν within the radius 2^l.

a. Interference terms in the density

The Wilson states $\psi_\nu(x)$ or $c_\nu^\dagger$ represent the free electron states in the impurity, problem. With the impurity, we express the ground state in terms of new states $a_i^\dagger = \Sigma_{\nu=0}^{N-1} \alpha_i^\nu c_\nu^\dagger$. Their integrated density is given by

$$\bar{\rho}_i(2^l) = \int_0^{2^l} \left| \sum_{\nu=0}^{N-1} \alpha_i^\nu \psi_\nu(x) \right|^2 dx.$$

The quadratic terms can be evaluated with the same ruler $I(s)$ as before. However, this time, one has in addition interference terms $\psi_\nu(x)\psi_{\nu+\lambda}(x)$. These terms depend on two parameters, ν and λ. So, one needs for each λ a different ruler. Furthermore, the interference terms depend on the subbands of $\psi_\nu(x)$ and $\psi_{\nu+\lambda}(x)$. If both states lie either in the negative energy subband $(\nu, \nu+\lambda < N/2)$ or in the positive subband $(\nu, \nu-\lambda \geqslant N/2)$, then one obtains one set of rulers $I_0(\nu,\lambda)$, and if they lie in opposite subbands, then one obtains another set of rulers $I_1(\nu,\lambda)$. As an example, one obtains

$$I_0(s,\lambda) = 2\sqrt{2^\lambda}\int_0^{2^s} \frac{\sin(\pi u)\sin\left(\pi\frac{u}{2^\lambda}\right)}{(\pi u)^2}\cos\left[3\pi u\left(1-\frac{1}{2^\lambda}\right)\right]du.$$

For $I_1(\nu,\lambda)$, one has to replace the minus sign in the cosine function by a plus sign. Furthermore, one has to treat the terms where $\nu+\lambda=N/2-1$ separately because one state lies at the Fermi level and has a different cell width.

b. Net integrated density

If we occupy all Wilson states below the Fermi level, then we obtain $\prod_{\nu=0}^{n-1} c_\nu^\dagger \Phi_0$, with $n=N/2$ and Φ_0 the vacuum state. This state is not really the free electron ground state. To obtain the latter, we have also to occupy the states $\overline{\varphi_k(x)}$ and $\overline{\overline{\varphi_k(x)}}$. They do not interact with the impurity but they are occupied. Therefore, we define as quasivacuum Φ_0' the state in which all states $\overline{\varphi_k(x)}$ and $\overline{\overline{\varphi_k(x)}}$ with $k<k_F=1$ are occupied. Then, the ground state is $\Psi_0=\prod_{\nu=0}^{n-1} c_\nu^\dagger \Phi_0'$. This state has a constant electron density in real space.

In the presence of the impurity, the new ground state must also contain this quasivacuum, i.e., the noninteracting states must be occupied up to the Fermi level. Since the inert states are occupied in Ψ_0 and Ψ_{new}, they cancel out when one calculates the change in the electron density. Since the inert states cancel out, one can ignore their existence during this calculation.

*bergmann@usc.edu

[1] J. Friedel, Philos. Mag. **43**, 153 (1952); Adv. Phys. **3**, 446 (1954); Philos. Mag., Suppl. **7**, 446 (1954); Can. J. Phys. **34**, 1190 (1956); Nuovo Cimento, Suppl. **7**, 287 (1958); J. Phys. Radium **19**, 38 (1958).
[2] P. W. Anderson, Phys. Rev. **124**, 41 (1961).
[3] J. Kondo, Prog. Theor. Phys. **32**, 37 (1964).
[4] K. Yosida, Phys. Rev. **147**, 223 (1966).
[5] C. M. Varma and Y. Yafet, Phys. Acoust. **13**, 2950 (1976).
[6] K. Schoenhammer, Phys. Rev. B **13**, 4336 (1976).
[7] M. D. Daybell and W. A. Steyert, Rev. Mod. Phys. **40**, 380 (1968).
[8] A. J. Heeger, in *Solid State Physics*, edited by F. Seitz, D. Turnbull, and H. Ehrenreich (Academic, New York, 1969), Vol. 23, p. 284.
[9] M. B. Maple, in *Magnetism*, edited by G. T. Rado and H. Suhl (Academic, New York, 1973), Vol. V, p. 289.
[10] P. W. Anderson, Rev. Mod. Phys. **50**, 191 (1978).
[11] G. Gruener and A. Zavadowski, Prog. Low Temp. Phys. **7B**, 591 (1978).
[12] P. Coleman, J. Magn. Magn. Mater. **47**, 323 (1985).
[13] A. C. Hewson, *The Kondo Problem to Heavy Fermions* (Cambridge University Press, Cambridge, 1993).
[14] P. W. Anderson, J. Phys. C **3**, 2436 (1970).
[15] K. G. Wilson, Rev. Mod. Phys. **47**, 773 (1975).
[16] H. O. Frota and L. N. Oliveira, Phys. Rev. B **33**, 7871 (1986).
[17] H. R. Krishna-murthy, J. W. Wilkins, and K. G. Wilson, Phys. Rev. B **21**, 1003 (1980).
[18] H. R. Krishna-murthy, J. W. Wilkins and K. G. Wilson, Phys. Rev. B **21**, 1044 (1980).
[19] P. Nozieres, J. Low Temp. Phys. **17**, 31 (1974).
[20] P. Nozieres, Ann. Phys. (Paris) **10**, 19 (1985).
[21] D. M. Newns and N. Read, Adv. Phys. **36**, 799 (1987).
[22] O. Gunnarsson and K. Schonhammer, Phys. Rev. B **28**, 4315 (1983).
[23] N. E. Bickers, Rev. Mod. Phys. **59**, 845 (1987).
[24] P. B. Wiegmann, in *Quantum Theory of Solids*, edited by I. M. Lifshits (MIR, Moscow, 1982), p. 238.
[25] N. Andrei, K. Furuya, and J. H. Lowenstein, Rev. Mod. Phys. **55**, 331 (1983).
[26] P. Schlottmann, Phys. Rep. **181**, 1 (1989).
[27] P. Nozieres and A. Blandin, J. Phys. (Paris) **41**, 193 (1980).
[28] J. B. Boyce and C. P. Slichter, Phys. Rev. Lett. **32**, 61 (1974).
[29] I. Affleck and P. Simon, Phys. Rev. Lett. **86**, 2854 (2001).
[30] I. Affleck, Proceedings of the NATO ASI on Field theory of Strangly Correlated Fermions and Bosons in Low-Dimensional Disordered Systems, Windsor, August 2001 (unpublished).
[31] R. G. Pereira, N. Laflorencie, I. Affleck, and B. I. Halperin, arXiv:cond-mat/0612635 (unpublished).
[32] L. Borda, Phys. Rev. B **75**, 041307(R) (2007).
[33] J. Simonin, arXiv:0708.3604 (unpublished).
[34] G. Bergmann, Z. Phys. B: Condens. Matter **102**, 381 (1997).
[35] G. Bergmann, Eur. Phys. J. B **2**, 233 (1998).
[36] G. Bergmann, Phys. Rev. B **73**, 092418 (2006).
[37] G. Bergmann, Phys. Rev. B **74**, 144420 (2006).
[38] G. Bergmann and L. Zhang, Phys. Rev. B **76**, 064401 (2007).
[39] O. Gunnarsson and K. Schoenhammer, Phys. Rev. B **31**, 4815 (1985).
[40] J. R. Schrieffer and P. A. Wolff, Phys. Rev. **149**, 491 (1967).
[41] G. Bergmann, arXiv:cond-mat/061020 (unpublished).
[42] G. Bergmann, Phys. Rev. Lett. **67**, 2545 (1991).